

Pareto fronts and trade-off relations from exact multi-objective optimization of thermal machines

José A. Almanza-Marrero¹, Édgar Roldán², Gonzalo Manzano^{1*}

¹Institute for Cross-Disciplinary Physics and Complex Systems, (IFISC, UIB-CSIC),

Campus Universitat de les Illes Balears E-07122, Palma de Mallorca, Spain.

²ICTP – The Abdus Salam International Centre for Theoretical Physics, Strada Costiera 11, 34151 Trieste, Italy

*Corresponding author. Email: gonzalo.manzano@ifisc.uib-csic.es

Thermal machines are physical systems that, when fueled by input energy, perform output tasks such as heat pumping or the production of work. Their performance is characterized with several, often competing quantities, such as power, efficiency, energy waste, and resilience to environmental noise. Multi-objective optimization provides a key tool to investigate the characterization of the best thermal machines operating in the irreversible linear-response regime. Here, we derive exact analytical parameterizations for the optimal (Pareto) fronts associated with any given choice of relative weights assigned to their mean extracted power P , efficiency η , entropy production Σ and the amplitude of power fluctuations σ_p^2 . The geometry of the front of endoreversible machines is universal: two-, three-, and four-objective trade-offs follow analytical formulae that do not depend on the value of any physical parameter of the machine. We show that such universal thermodynamic Pareto fronts also set quantitative fundamental limits for the performance of non-endoreversible machines. Furthermore, we demonstrate that our results apply to existing experimental data from different physical systems also beyond the linear regime, ranging from atomic to macroscopic scales, including single-atom engines, colloidal systems, macroscopic engines and power plants.

1 Introduction

Mankind has over centuries sought to understand how natural resources can be used efficiently to run thermal machines that convert one type of energy (e.g. potential) into another (e.g. kinetic). A key example that dates back from the medieval age is a windmill operated by the flow of wind, enabling to pump water, mill grain, or develop other functions, such as the generation of electricity as in wind turbines developed in the 20th century. A pertinent fundamental and applied question is what the optimal design principles are (e.g. how many vanes and how large each) to optimize the performance of a machine (e.g. to maximize the rate of water pumping) for a prescribed value of the resources (e.g. the speed of the wind flow). Tackling this question has devoted the efforts of thousands of scientists and engineers over the last centuries employing the framework of thermodynamics.

Carnot's pioneering work in the 18th century marked the birth of modern thermodynamics (1). Carnot was driven by simple yet profound questions: what makes one heat engine better than another? What limits does nature impose on machines that convert her resources into motion? He discovered that such machines are subject to fundamental constraints that cannot be overcome. Consider, for instance, a steam engine operating between a hot source and a cold sink: it can only approach its maximum possible efficiency—the Carnot efficiency—if it runs extremely slowly, almost quasistatically, yielding zero power in the ideal limit. Pushing the machine to run faster increases its power output, but also inevitably increases the amount of energy dissipated (2).

From Carnot's discoveries to contemporary analysis of machines on the nanoscale, the relationship between maximum efficiency and maximum power regimes has been studied extensively (3, 4, 5, 6, 7, 8, 9, 10). In parallel, technological advances over the past few decades have brought access to manipulation of natural and artificial microscopic machines with exquisite accuracy, ranging from single atoms (11, 12) to molecular motors (13, 14, 15). Small machines also obey power–efficiency and power–dissipation trade-offs like macroscopic machines, but with an additional constraint: they must operate reliably in the presence of fluctuations of different origin (thermal, chemical, etc.) present in their surrounding environment (16, 17, 18, 19, 20).

A natural way to tackle competing objectives is through the so-called multi-objective (so-called *Pareto*) optimization. This idea originally emerged in economics (21), where one seeks to balance

different goals—such as cost and quality—by assuming that any desired output can be maximized while compromising at least one of the others through trade-off relations. Although Vilfredo Pareto’s socio-economic study (22) did not explore or venture trade-off relations to be applicable in the natural sciences, Pareto optimization has emerged as a powerful technique, finding widespread applications in miscellaneous disciplines such as engineering, biology, computer science, and evolutionary theory (23, 24). In thermodynamics, optimization approaches are increasingly being used in a wide range of contexts, including inference, enhancement of free-energy harvesting, or optimal control at the microscale (25, 26, 27). In this context, multi-objective optimization offers a powerful framework to characterize trade-offs between thermodynamic quantities that typically compete with one another (28, 29, 30, 31, 32). The main idea is rather intuitive: instead of searching for a single “best” machine, one identifies those designs that cannot be improved in one performance metric—say, power—without compromising another performance metric, such as efficiency, dissipation, or precision. When all such possibilities are considered, they form what is known as a Pareto front. From this perspective, thermodynamic trade-offs provide the appropriate framework to establish the boundaries of machines’ performance limits (see Fig. 1a).

In this work, we derive the exact optimal trade-off relations between power, efficiency, dissipation, and precision for generic thermal machines operating in the linear irreversible response regime (33, 34). We find that for endoreversible machines (the class originally considered by Carnot) these optimal relations are universal, and take the form of rather compact analytical expressions. Beyond the familiar results of maximum power and Carnot efficiency, all other optimal quantities turn out to be independent of the specific physical details of the machine. Moreover, we show that this class of thermal machines sets the ultimate limits of what is thermodynamically achievable for all other machines. Together with the mathematical simplicity of our results, this universality greatly enhances their potential applications. As a matter of fact, we validate these theoretical results using experimental data existing in the literature from different platforms across scales, ranging from single-atom engines to power plants, and operating even beyond the linear regime.

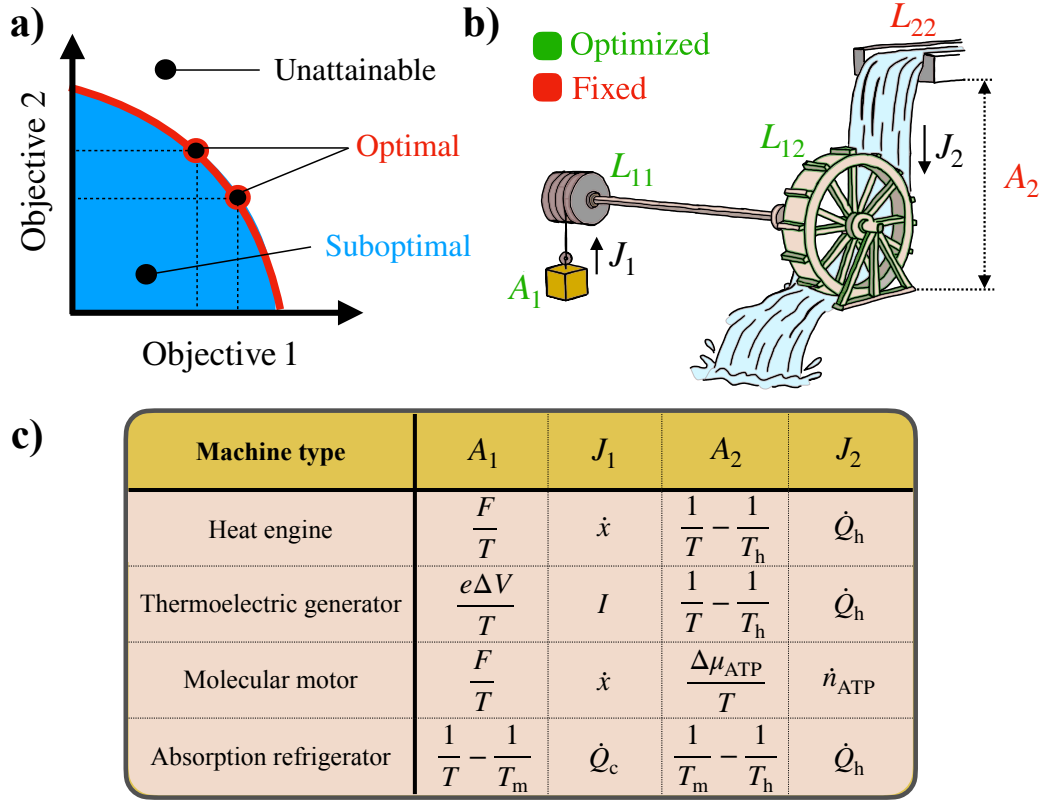


Figure 1: (a) Sketch of a multi-objective optimization for the case of two objectives. The blue region represents the permitted values for the two objectives while the white region represents unattainable configurations. The red solid line at the frontier between the two regions corresponds to optimal configurations (the so-called *Pareto* front). The Pareto front quantifies a trade-off relation inasmuch if one wants to increase one objective then the other objective's value has to decrease. (b) Sketch of an example multi-objective optimization in a windmill (in the linear-response regime), where we keep the quantities A_2 (the height of the waterfall) and L_{22} (the rate of water flow of the river atop the waterfall) fixed, as they represent the thermodynamic resources available to the windmill. The quantities varied are A_1 (the weight of the load), L_{11} (the effectivity of the pulley mechanism) and L_{12} (the effectivity of the windmill blades). (c) Onsager affinities A_1 , A_2 and their conjugate fluxes J_1 , J_2 for different thermal machines. Here F is an external force, \dot{x} the linear velocity, e the elementary charge, ΔV the electrical potential difference, I the electric current, $\Delta\mu_{\text{ATP}}$ the chemical potential difference per ATP, and \dot{n}_{ATP} the ATP consumption rate. The symbols T_h , and T_m denote hot and intermediate reservoir temperatures, while \dot{Q}_h and \dot{Q}_c are the heat fluxes from the respective reservoirs.

2 Linear irreversible thermodynamics in a nutshell

Thermal machines often operate by exploiting spatial or temporal inhomogeneities of physical quantities such as temperature, chemical potential, or pressure. Such gradients induce thermodynamic forces, denoted here by A , which drive the machine out of equilibrium. Each force is associated with a conjugate flux J , such as heat or particle currents. The main goal of a thermal machine is to convert one type of energy (e.g. heat) into another type (e.g. work). In the simplest scenario, this conversion requires at least two forces: a load (input) force A_1 against which useful work is performed, and a driving (output) force A_2 which supplies energy to the system. The working regime is characterized by the sign of the fluxes: an entropy-producing flux in the direction of the driving force, $A_2 J_2 \geq 0$, sustains the other flux against the load force, $A_1 J_1 \leq 0$.

In this context, one of the key quantities of interest is the average power extracted from the machine P , that is, the work that the load force is able to produce per unit time. Within this framework, it can be defined as (6)

$$P = -T A_1 J_1, \quad (1)$$

where T is a reference temperature of the power-producing device (35). See Fig. 1c for some prototypical examples of thermal machines and their associated fluxes and forces.

Another of the key quantities in any thermodynamic process is the rate of dissipation Σ given by the rate of entropy production, which in the linear-response regime can be expressed as a combination of fluxes and forces (33, 34)

$$\Sigma = A_1 J_1 + A_2 J_2 \geq 0, \quad (2)$$

where the last inequality enforces the second law of thermodynamics. From the second law, it is also natural to introduce a measure of efficiency $\bar{\eta}$ of the machine

$$\bar{\eta} = -\frac{A_1 J_1}{A_2 J_2}, \quad (3)$$

which captures the fraction of entropy flux that is used to generate power. The working regime is characterized by both positive power extraction and efficiency. In addition, the second law implies that, in the working regime, $\bar{\eta} \leq 1$. The maximum efficiency $\bar{\eta} = 1$, is reached in the reversible

limit corresponding to zero dissipation $\Sigma = 0$.¹

When forces are small, fluxes respond linearly, and Onsager theory holds, $\vec{J} = \mathbb{L}\vec{A}$, (36)

$$\begin{pmatrix} J_1 \\ J_2 \end{pmatrix} = \begin{pmatrix} L_{11} & L_{12} \\ L_{21} & L_{22} \end{pmatrix} \begin{pmatrix} A_1 \\ A_2 \end{pmatrix}, \quad (4)$$

where the matrix elements L_{ij} in \mathbb{L} are known as Onsager coefficients. The second law of thermodynamics [Eq. (2)] constrains \mathbb{L} to be positive semi-definite, which sets: $L_{11} \geq 0$, $L_{22} \geq 0$, and $(L_{11} + L_{22})^2 \leq 4L_{12}L_{21}$. Under time-reversal symmetry conditions (e.g. in absence of magnetic fields), \mathbb{L} is symmetric, leading to the celebrated Onsager reciprocity $L_{12} = L_{21}$. If additionally one has degeneracy $L_{12}^2 = L_{11}L_{22}$ in the Onsager coefficients, the two currents become proportional, enabling the machine to approach reversibility (Carnot's bound) at vanishing dissipation. The machines verifying the additional property $L_{12}^2 = L_{11}L_{22}$ are called endoreversible machines (37).

Moreover, on mesoscopic scales, fluctuations in the currents play a fundamental role. Within the linear response regime, the fluctuation–dissipation theorem (37) relates current variances to the Onsager coefficients, implying that the equilibrium variance of each current satisfies $\langle J_i^2 \rangle_{\text{eq}} = 2L_{ii}$. Under the standard assumption that forces are externally imposed and effectively nonfluctuating (differences in temperatures, chemical potentials, etc), the output-power variance, $\sigma_P^2 = \langle P^2 \rangle - \langle P \rangle^2$ obeys

$$\sigma_P^2 = A_1^2 T^2 \sigma_{J_1}^2 = 2T^2 A_1^2 L_{11}, \quad (5)$$

where we have used $\sigma_{J_1}^2 = \langle J_1^2 \rangle_{\text{eq}} - \langle J_1 \rangle_{\text{eq}}^2$ and $\langle J_1 \rangle_{\text{eq}} = 0$. Notably, Eq. (5) allows treating σ_P^2 on the same footing as the other performance metrics P , η , and Σ in multi-objective optimization analysis.

3 Multi-objective optimization of thermal machines

In his original work, Carnot thought of heat engines as water mills driven by a waterfall, where the falling water represented heat flowing from one reservoir to another. To define our optimization problem, we adopt a closely related picture within the framework of linear thermodynamics (see

¹For heat engines, the reversible limit is associated with the Carnot limit, since in that case $J_2 = Q_h$ is the input heat from a hot source at T_h and $A_2 = 1/(T_h - T)$ is the inverse temperature difference, leading to the energetic efficiency $\eta_e \equiv \frac{P}{Q_h} = \bar{\eta} \left(1 - \frac{T}{T_h}\right) \leq \eta_C$, which reaches Carnot's bound $\eta_C = 1 - (T/T_h)$ for $\bar{\eta} = 1$.

Fig. 1b). How would the quantities introduced in the previous section appear in Carnot's picture? First, there is the affinity that allows work to be extracted, denoted by A_2 , which in this analogy corresponds to the height of the waterfall—the drop through which the water falls. This affinity has an associated flux, J_2 , represented by the stream of water flowing down the cascade itself. Together, these resources set the mill into motion and allow it to perform a useful task, such as lifting a heavy load. The weight of this load represents the second affinity, A_1 , associated with the work performed by the engine, while its corresponding flux, J_1 , is the speed at which the load is lifted.

As discussed earlier, within linear-response thermodynamics all these quantities are related through the Onsager coefficients L_{ij} , which encode how affinities and fluxes are coupled. In this picture, L_{22} represents the rate of water flow of the river atop the waterfall, while L_{12} quantifies how efficiently the mill can exploit this resource—that is, how well its blades convert falling water into motion. Finally, L_{11} measures the efficiency of the pulley mechanism, determining how easily the motion of the mill can be converted to lifting the load. From this perspective, our choice of optimization variables becomes natural: throughout this work we keep L_{22} and A_2 fixed, as they represent the thermodynamic resources available to the machine.

This choice is rather intuitive—we cannot choose the river that feeds the waterfall or its height, but we are free to design the mill itself.

3.1 Optimal performance of endoreversible thermal machines

We first focus on endoreversible machines, that is, those verifying Onsager reciprocity $L_{12} = L_{21}$ and $L_{12}^2 = L_{11}L_{22}$, which are capable of reaching the Carnot limit. In order to address the joint optimization of efficiency, dissipation, mean power, and power fluctuations, we employ a weighted-sum scalarization, where a parametrization with three independent weights $0 \leq \alpha \leq 1$, $0 \leq \beta \leq 1$, and $0 \leq \gamma \leq 1$ is introduced, together with a fourth weight $1 - \alpha - \beta - \gamma$ that ensures normalization. We then proceed to the optimization of a single objective function of the form

$$\Omega(\alpha, \beta, \gamma) = \alpha \bar{P} + \beta \bar{\eta} - \gamma \bar{\Sigma} - (1 - \alpha - \beta - \gamma) \overline{\sigma_P^2}, \quad (6)$$

where the minus sign stands for the thermodynamic quantities that have to be minimized and we have $\bar{P} = P/P_{\max}$, $\bar{\eta} = \eta/\eta_{\max}$, $\bar{\Sigma} = \Sigma/\Sigma_{\max}$ and $\overline{\sigma_P^2} = \sigma_P^2/\sigma_{P,\max}^2$ being the thermodynamic quantities normalized by their respective global maxima. For the class of thermal machines studied

here, the maximal values of mean power, dissipation, and power fluctuation depend only on A_2 , L_{22} and T ; they read $P_{\max} \equiv \max(P) = TA_2^2L_{22}/4$, $\Sigma_{\max} \equiv \max(\Sigma) = A_2^2L_{22}$, and $\sigma_{P,\max}^2 \equiv \max(\sigma_P^2) = 2T^2A_2^2L_{22}$. Maximizing Ω in Eq. (6) is a weighted joint optimization problem towards maximum power, maximum efficiency, minimum dissipation and minimum power fluctuations.

By scanning the weights in the simplex $\alpha + \beta + \gamma \leq 1$, we obtain a family of optimal solutions in which every parameter value yields the relative weight associated with a specific thermodynamic quantity — α for the mean power, β for the efficiency and γ for the dissipation. We solve this multi-objective optimization problem for all values of α , β and γ in the simplex by maximizing Ω with respect to A_1 and L_{11} while fixing the available thermodynamic resources (L_{22} and A_2) since all (maximum) performance metrics scale linearly with them. We show that the analytical expression of the full parametric solution of this multi-objective problem is given by

$$\bar{P}^*(\alpha, \beta, \gamma) = -\frac{12(\beta - 1)(\alpha - \gamma + 1)(\alpha(\beta + 6) - \beta\gamma + \beta + 3\gamma)}{(\alpha(9 - 2\beta) + 2\beta(\gamma - 1) + 3)^2}, \quad (7)$$

$$\bar{\eta}^*(\alpha, \beta, \gamma) = \frac{\alpha(\beta + 6) - \beta\gamma + \beta + 3\gamma}{\alpha(9 - 2\beta) + 2\beta(\gamma - 1) + 3}, \quad (8)$$

$$\bar{\Sigma}^*(\alpha, \beta, \gamma) = \frac{9(\beta - 1)^2(\alpha - \gamma + 1)^2}{(\alpha(9 - 2\beta) + 2\beta(\gamma - 1) + 3)^2}, \quad (9)$$

$$\bar{\sigma}_P^2(\alpha, \beta, \gamma) = \frac{(\alpha(\beta + 6) - \beta\gamma + \beta + 3\gamma)^2}{(\alpha(9 - 2\beta) + 2\beta(\gamma - 1) + 3)^2}. \quad (10)$$

Equations (7)–(10) describe the optimal performance surface (Pareto front) on the four-dimensional manifold of power, efficiency, dissipation and power fluctuations. Strikingly, the shape of the optimal solutions does not depend on any physical detail of our system, but it is only dictated by a non-linear combination of the optimization weights. In other words, within the linear regime and under endoreversible operation, the optimal (multi-objective) compromises between the main thermodynamic performance quantifiers of the machine are described by a universal, model-independent relation. Setting one or more weights to zero effectively removes the associated thermodynamic quantities from the optimization problem and projects the four-dimensional Pareto front in Eq. (7)–(10) into three-dimensional or two-dimensional spaces. As a consequence, the complete parametric solution of the optimization problem in Eqs. (7–10) connects smoothly to lower-dimensional tradeoffs of the main thermodynamic quantities, as the ones reported in Fig. 2 a-f.

An alternative insightful perspective of the results given by Eqs. (7–10) is to write the solutions

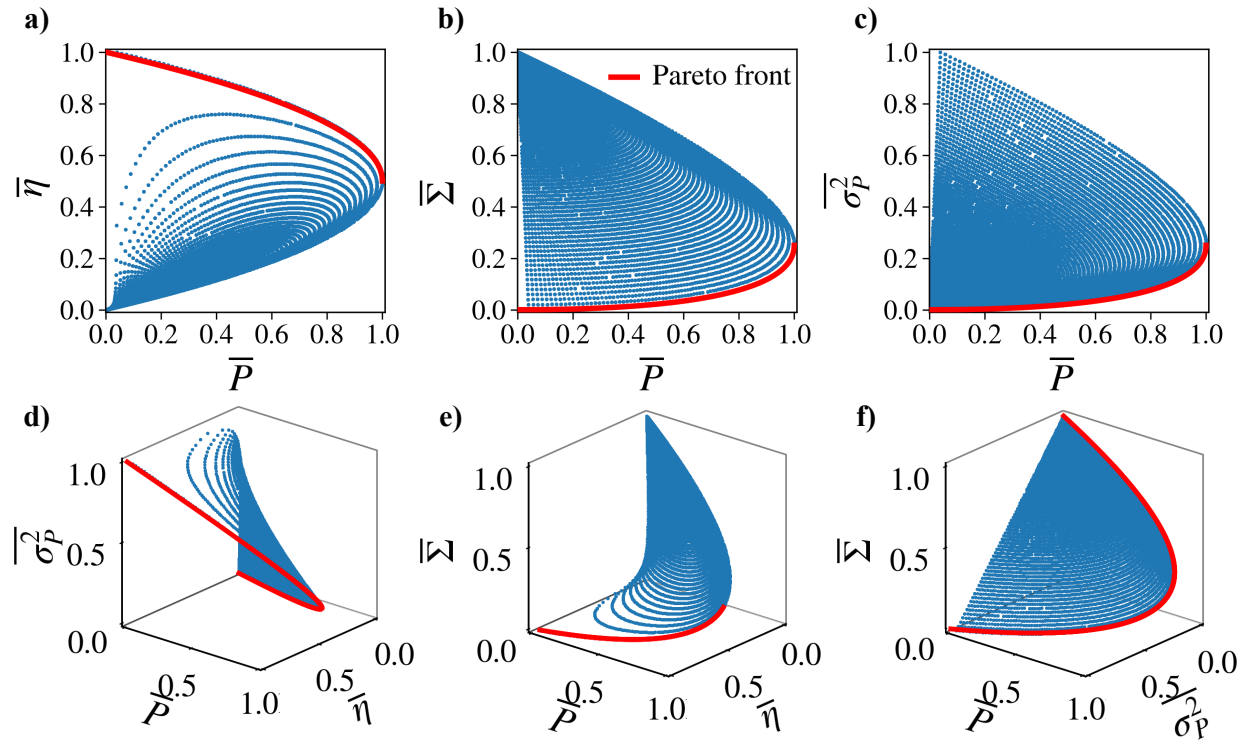


Figure 2: Pareto fronts (red solid lines) derived in this work in two (a-c) and three (d-f) dimensional spaces (see Sec. 3.1 for more details). The blue points are configurations in the linear regime with parameters: $A_2 = 1$, $L_{22} = 1$.

explicitly and interpret them as inequalities, with equality corresponding to optimal operation, i.e. over the Pareto front. From this perspective, the bounds are not merely mathematical statements but quantitative expressions of physical limits (38, 39). We eliminate the parametric dependence on (α, β, γ) by substitution, leaving direct relations between physical quantities. For example, projecting the multi-objective solution [Eqs. (7)–(10)] onto two-dimensional subspaces yields the following inequalities for the power–efficiency ($\gamma = 0$ and $\beta = 1 - \alpha$), power–dissipation ($\beta = 0$ and $\gamma = 1 - \alpha$), and power–fluctuation ($\gamma = 0$ and $\beta = 0$) trade-offs

$$\bar{\eta} \leq \frac{1 + \sqrt{1 - \bar{P}}}{2}, \quad \bar{\Sigma} \geq \frac{(1 - \sqrt{1 - \bar{P}})^2}{4}, \quad \overline{\sigma_P^2} \geq \frac{(1 - \sqrt{1 - \bar{P}})^2}{4}. \quad (11)$$

The right-hand side of each inequality represents the best possible performance, acting as either an upper bound (if we are maximizing the quantity) or a lower bound (if we are minimizing the quantity). For example, the first inequality above sets the efficiency at (unconstrained) maximum power ($\bar{P} = 1$) to be universally bounded by half of the maximum efficiency, $\bar{\eta}_{MP} \leq 1/2$, as first noticed in Ref. (6), and predicts a square-root dependency of the maximal efficiency as a function of the 'sacrificed' power $1 - \bar{P}$, see Fig. 2a for numerical tests. On the other hand, the second and third inequalities set the minimum values $\bar{\Sigma}_{MP} \geq 1/4$ and $\overline{\sigma_{P,MP}^2} \geq 1/4$ for dissipation and power fluctuations at maximum power, which may be reduced through a non-linear relation with the amount of sacrificed output power $1 - \bar{P}$ (Fig. 2b and c). Among other potential implications, we observe that no output power is possible $\bar{P} \leq 0$ at maximum efficiency ($\bar{\eta} = 1$), zero dissipation ($\bar{\Sigma} = 0$) or zero power fluctuations ($\overline{\sigma_P^2} = 0$). Indeed, negligible fluctuations may only be achieved at zero power. Inequalities (11) generalize previous insights on maximum power, maximum efficiency, and minimum dissipation derived in the linear regime in Refs. (6, 10, 40, 41) by both including fluctuations and providing a whole family of optimal compromises between the performance metrics of interest.

Our analytical formulae permits tackling the more challenging scenario of the three-dimensional trade-offs shown in Fig. 2e–f. In this case, we obtain the corresponding inequalities that describe universal power-efficiency-fluctuations ($\gamma = 0$), power-dissipation-fluctuations ($\beta = 0$), and power-efficiency-dissipation ($\gamma = 1 - \alpha - \beta$) trade-offs:

$$\frac{\bar{P}}{\sigma_P^2} \frac{\bar{\eta}}{1 - \bar{\eta}} \leq 4, \quad \bar{\Sigma} \frac{\overline{\sigma_P^2}}{\bar{P}^2} \geq \frac{1}{16}, \quad \bar{\Sigma} \frac{\bar{\eta}^2}{\bar{P}^2} \geq \frac{1}{16}. \quad (12)$$

Using the relations between the maximal thermodynamic quantities for endoreversible heat engines, $\Sigma_{\max} = 4P_{\max}/T$ and $\sigma_{P,\max}^2 = 8TP_{\max}$, we can recast these bounds in terms of unnormalized quantities, obtaining

$$T \frac{P}{\sigma_P^2} \left(\frac{\eta}{\eta_{\max} - \eta} \right) \leq \frac{1}{2}, \quad \Sigma \frac{\sigma_P^2}{P^2} \geq 2, \quad \Sigma \geq \frac{P^2}{4TP_{\max}} \left(\frac{\eta_{\max}}{\eta} \right)^2, \quad (13)$$

where the first and second inequalities in Eq. (13) correspond to two analogous formulations of the so-called thermodynamic uncertainty relation TUR², discussed respectively in Refs. (42) and (19, 20). The TUR implies that improving the accuracy of the output power (i.e. lowering the fluctuations for a given output power) can only be achieved at the cost of increasing the dissipation or sacrificing efficiency. On the other hand, the third inequality (a lower bound of the dissipation in terms of a quadratic function of power over the efficiency) implies that the dissipation of the machine may be reduced by either decreasing in the output power or by approaching the maximum efficiency. This result has remained elusive in the literature to the best of our knowledge. By definition, the bounds on Eqs. (12)–(13) are saturated only by the optimal configurations (i.e. those on the Pareto front), thus saturating the TUR is optimal in the linear response limit. Moreover, the parametric solutions obtained from the different optimization schemes identify the specific ways of approaching the optimal limit, depending on how power, efficiency, dissipation, and fluctuations are weighted. Taken together, our results thus provide a linear-response derivation of the thermodynamic uncertainty relation as the natural outcome of optimal trade-offs involving power fluctuations.

3.2 Endoreversible thermal machines as the limit of performance

In an endoreversible heat engine, heat and work-producing fluxes are perfectly coupled, i.e. every unit of heat transferred is converted directly into useful work. However, in real systems, internal irreversibilities weaken this coupling. Deviations from the endoreversible limit stem, for example, from imperfect coupling between fluxes. That is the case of thermoelectric generators where the electrical current (work flux) and heat flow are ideally linked through the Seebeck effect, but parasitic heat conduction allows heat to flow without generating electrical power. Likewise, in mechanical heat engines, friction, turbulence, finite-rate heat transfer, or fluid leakage cause part of the energy

²Notably, if we try to obtain the explicit expression for the full optimization problem [Eqs. (7)–(10)], the second inequality in Eq. (13) [$\Sigma\sigma_P^2/P^2 \geq 2$] is recovered again.

flow to dissipate as waste rather than being converted into useful work. These leakages reduce the degree of coupling between fluxes and therefore drive the system away from the endoreversible limit. In the Supplementary Materials, we prove that any reciprocal thermal machine ³ in the linear-response must satisfy the following point-wise bounds when A_1 , A_2 , L_{11} , and L_{22} are fixed

$$P(q < 1) \leq P_{\text{endo}}(q = 1), \quad \eta(q < 1) \leq \eta_{\text{endo}}(q = 1), \quad \Sigma(q < 1) \geq \Sigma_{\text{endo}}(q = 1), \quad (14)$$

where we introduce the dimensionless coupling parameter $q = |L_{12}|/\sqrt{L_{11}L_{22}}$, and use the label “endo” to denote the corresponding values for endoreversible operation. These inequalities become equalities only under perfect coupling ($q = 1$) or in the trivial zero-power limit. Consequently, the universal optimal fronts in Eq. (7)–(10), derived for endoreversible machines, represent the ultimate thermodynamic performance boundaries for any machine obeying Onsager reciprocity. Furthermore, we find that these bounds remain valid even when Onsager reciprocity is broken, provided the asymmetric coefficients of the Onsager matrix \mathbb{L} satisfy $|L_{12}|, |L_{21}| \leq \sqrt{L_{11}L_{22}}$.

4 Optimal performance of real-world thermal machines

The analytical simplicity of our results, combined with their independence from system-specific details, enables their application to a broad range of real-world machines. In this section, we put our findings to the test across scales—from microscopic to macroscopic systems—and across operational regimes ranging from low dissipation to strongly nonequilibrium conditions. Figure 3 displays the optimal trade-offs predicted by Eq. (11) as a red solid line. The symbols are obtained through a thorough survey of existing experimental data from different platforms: a single-atom engine composed of a cesium impurity embedded in an ultra-cold rubidium gas (12); an Otto cycle implemented in a liquid-state Nuclear Magnetic Resonance platform using the nuclear spin of a carbon-13 nucleus in a chloroform molecule (43); a Brownian heat engine using a single colloidal particle trapped by optical tweezers in a fluid and driven by two phase-shifted periodic forces (40); an experimental implementation of a macroscopic finite-time Carnot cycle using dry air inside a piston (44); and recently reported performance data from several generations of nuclear power plants (45).

³We refer to reciprocal thermal machines as those machines that satisfy the Onsager reciprocity condition $L_{12} = L_{21}$.

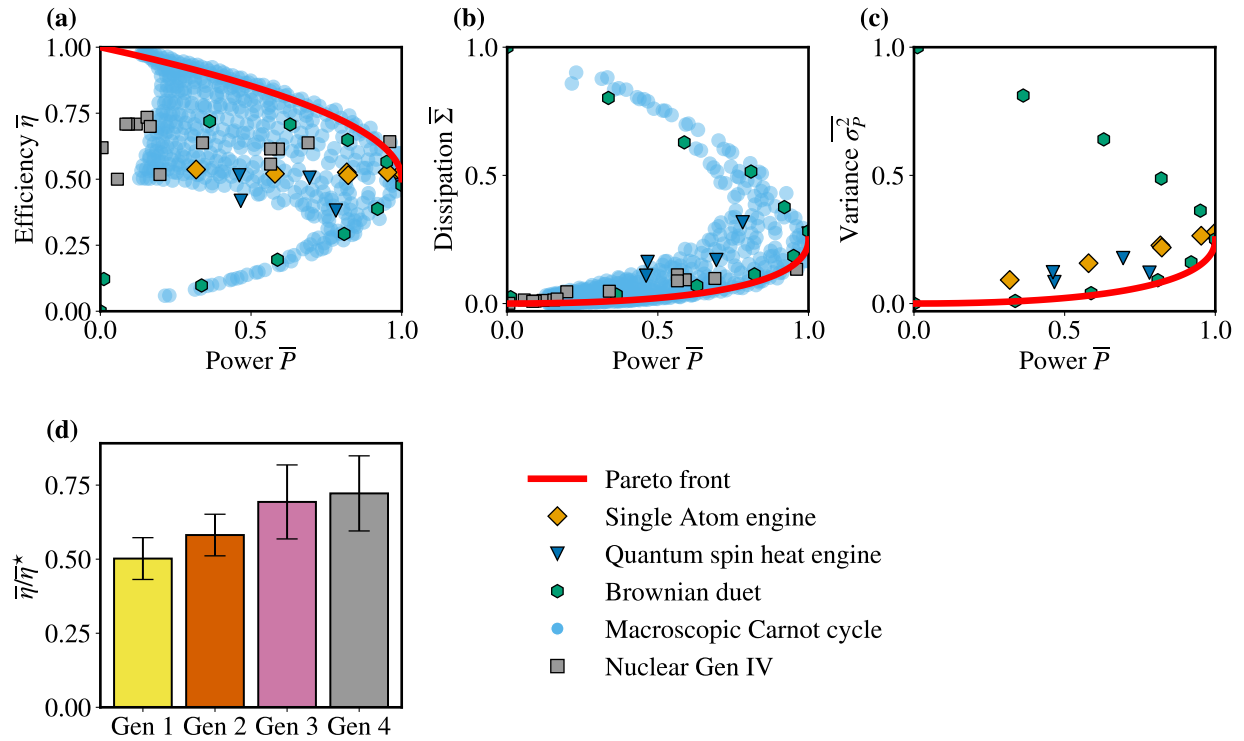


Figure 3: (a–c) Pareto fronts (red solid lines) derived in this work for the two-dimensional trade-offs considered. Symbols correspond to experimental data from different systems, as specified in the legend. (d) Bar plot of the ratio of the achieved efficiency to the optimal efficiency for different generations of nuclear power plants. For each generation, values are obtained by averaging over individual plants, with error bars indicating the corresponding standard deviations.

Across the three performance trade-offs shown in Fig. 3(a-c), we find a consistent hierarchy in how closely different engines approach optimal operation. Finite-time Carnot cycle implementation uniquely span the full optimal-performance branches in the power-efficiency and power-dissipation cases, while the Brownian engine and the last generation nuclear power plants systematically operate near all this corresponding optimal frontiers. Atomic engines display intermediate performance in the power–efficiency figure, and the quantum spin engine remains comparatively further from optimality in the power–dissipation trade-off. At mesoscopic scales where fluctuations are relevant, the Brownian engine again nearly saturates the optimal bound, with quantum engine implementations exhibiting similarly fluctuating behavior close to the optimal Pareto fronts.

Figure 3d illustrates the average distance to optimal performance of different generations of nuclear power plants, using data from Ref. (45). For each plant, we compute the fraction of the optimal efficiency achieved ($\bar{\eta}/\eta^*$) at its operating power and then average it for each generation of power plant, shown as bars in Fig. 3d, with the error bars given by their respective intra-generation standard deviations. Using this multiobjective optimization criterion, we find a systematic, statistically-significant improvement in performance across successive generations of nuclear power plants.

5 Conclusions

In this work, we introduced and solved analytically a multi-objective optimization framework to characterize the fundamental performance limits of thermal machines operating in the linear response regime. By jointly analyzing power, efficiency, dissipation, and power fluctuations, we derived exact analytical parametrizations of the corresponding Pareto fronts, which fully capture the optimal trade-offs among these competing thermodynamic objectives. A central outcome of our analysis is the identification of universal Pareto fronts for endoreversible machines. We showed that the geometry of these optimal performance boundaries is independent of microscopic details and depends only on the relative weighting of the optimized objectives. These universal fronts therefore set absolute performance limits for reciprocal thermal machines, with non-endoreversible systems necessarily operating below the ideal boundary.

We have put to the test our theoretical predictions with existing experimental data across a

wide range of physical scales, from microscopic and mesoscopic engines to macroscopic heat engines and power plants. The observed performance of these real-world thermal machines falls with striking accuracy within the predicted tradeoff limits. Notably, we observed a systematic across technological generations of nuclear power plants to progressively approach towards the universal optimal front. Altogether, our results demonstrate that multi-objective optimality provides a unifying and quantitative perspective for comparing thermal machines and for assessing how close machines operate to fundamental physical limits.

References and Notes

1. S. Carnot, Reflections on the Motive Power of Fire, and Other Papers on the Second Law of Thermodynamics (Dover Publications) (1960).
2. F. L. Curzon, B. Ahlborn, Efficiency of a Carnot engine at maximum power output. American Journal of Physics **43** (1), 22–24 (1975), doi:10.1119/1.10023.
3. I. Novikov, The efficiency of atomic power stations (a review). Journal of Nuclear Energy (1954) **7** (1), 125–128 (1958), doi:[https://doi.org/10.1016/0891-3919\(58\)90244-4](https://doi.org/10.1016/0891-3919(58)90244-4), <https://www.sciencedirect.com/science/article/pii/0891391958902444>.
4. R. Kosloff, A quantum mechanical open system as a model of a heat engine. The Journal of Chemical Physics **80** (4), 1625–1631 (1984), doi:10.1063/1.446862, <https://doi.org/10.1063/1.446862>.
5. H. S. Leff, Thermal efficiency at maximum work output: New results for old heat engines. American Journal of Physics **55** (7), 602–610 (1987), doi:10.1119/1.15071, <https://doi.org/10.1119/1.15071>.
6. C. Van den Broeck, Thermodynamic efficiency at maximum power. Physical Review Letters **95** (19), 190602 (2005), doi:10.1103/PhysRevLett.95.190602.
7. T. Schmiedl, U. Seifert, Efficiency at maximum power: An analytically solvable model for stochastic heat engines. Europhysics Letters **81** (2), 20003 (2008), doi:10.1209/0295-5075/81/20003.
8. M. Esposito, K. Lindenberg, C. Van den Broeck, Universality of Efficiency at Maximum Power. Phys. Rev. Lett. **102**, 130602 (2009), doi:10.1103/PhysRevLett.102.130602, <https://link.aps.org/doi/10.1103/PhysRevLett.102.130602>.
9. A. E. Allahverdyan, K. V. Hovhannisyanyan, A. V. Melkikh, S. G. Gevorkian, Carnot Cycle at Finite Power: Attainability of Maximal Efficiency. Phys. Rev. Lett. **111**, 050601 (2013), doi:10.1103/PhysRevLett.111.050601, <https://link.aps.org/doi/10.1103/PhysRevLett.111.050601>.

10. K. Proesmans, B. Cleuren, C. Van den Broeck, Power-Efficiency-Dissipation Relations in Linear Thermodynamics. Phys. Rev. Lett. **116**, 220601 (2016), doi:10.1103/PhysRevLett.116.220601, <https://link.aps.org/doi/10.1103/PhysRevLett.116.220601>.
11. J. Roßnagel, et al., A single-atom heat engine. Science **352** (6283), 325–329 (2016), doi:10.1126/science.aad6320, <https://www.science.org/doi/abs/10.1126/science.aad6320>.
12. Q. Bouton, et al., A quantum heat engine driven by atomic collisions. Nature Communications **12** (1) (2021), doi:10.1038/s41467-021-22222-z, <http://dx.doi.org/10.1038/s41467-021-22222-z>.
13. U. Seifert, Stochastic thermodynamics, fluctuation theorems and molecular machines. Reports on Progress in Physics **75** (12), 126001 (2012), doi:10.1088/0034-4885/75/12/126001.
14. V. Blickle, C. Bechinger, Realization of a micrometre-sized stochastic heat engine. Nature Physics **8** (2), 143–146 (2012), doi:10.1038/nphys2163.
15. I. A. Martínez, et al., Brownian Carnot engine. Nature Physics **12** (1), 67–70 (2015), doi:10.1038/nphys3518, <http://dx.doi.org/10.1038/nphys3518>.
16. C. Jarzynski, Nonequilibrium Equality for Free Energy Differences. Physical Review Letters **78** (14), 2690–2693 (1997), doi:10.1103/PhysRevLett.78.2690.
17. G. E. Crooks, Entropy production fluctuation theorem and the nonequilibrium work relation for free energy differences. Physical Review E **60** (3), 2721–2726 (1999), doi:10.1103/PhysRevE.60.2721.
18. C. Bustamante, J. Liphardt, F. Ritort, The nonequilibrium thermodynamics of small systems. Physics today **58** (7), 43–48 (2005).
19. A. C. Barato, U. Seifert, Thermodynamic uncertainty relation for biomolecular processes. Physical Review Letters **114** (15), 158101 (2015), doi:10.1103/PhysRevLett.114.158101.

20. T. R. Gingrich, J. M. Horowitz, N. Perunov, J. L. England, Dissipation Bounds All Steady-State Current Fluctuations. Phys. Rev. Lett. **116**, 120601 (2016), doi:10.1103/PhysRevLett.116.120601, <https://link.aps.org/doi/10.1103/PhysRevLett.116.120601>.
21. T. C. Koopmans, An analysis of production as an efficient combination of activities. Activity analysis of production and allocation (1951).
22. V. Pareto, The mind and society, vol. 1 (Harcourt, Brace and Company (New York)) (1935).
23. K. Deb, Multi-Objective Optimization Using Evolutionary Algorithms (Wiley) (2001).
24. L. F. Seoane, R. Solé, Phase transitions in Pareto optimal complex networks. Phys. Rev. E **92**, 032807 (2015), doi:10.1103/PhysRevE.92.032807, <https://link.aps.org/doi/10.1103/PhysRevE.92.032807>.
25. O. Movilla Miangolarra, A. Eldesoukey, A. Movilla Miangolarra, T. T. Georgiou, Maximum entropy inference of reaction–diffusion models. The Journal of Chemical Physics **162** (19) (2025), doi:10.1063/5.0256659, <http://dx.doi.org/10.1063/5.0256659>.
26. J. Piñero, R. Solé, A. Kolchinsky, Optimization of nonequilibrium free energy harvesting illustrated on bacteriorhodopsin. Phys. Rev. Res. **6**, 013275 (2024), doi:10.1103/PhysRevResearch.6.013275, <https://link.aps.org/doi/10.1103/PhysRevResearch.6.013275>.
27. S. A. M. Loos, S. Monter, F. Ginot, C. Bechinger, Universal Symmetry of Optimal Control at the Microscale. Phys. Rev. X **14**, 021032 (2024), doi:10.1103/PhysRevX.14.021032, <https://link.aps.org/doi/10.1103/PhysRevX.14.021032>.
28. T. Yilmaz, A new performance criterion for heat engines: efficient power. J. Energy Inst. **79** (1), 38–41 (2006).
29. C. de Tomás, A. C. Hernández, J. M. M. Roco, Optimal low symmetric dissipation Carnot engines and refrigerators. Physical Review E **85** (1), 010104 (2012), doi:10.1103/PhysRevE.85.010104.
30. Y. Ashida, T. Sagawa, Learning the best nanoscale heat engines through evolving network topology. Communications Physics **4** (1), 45 (2021).

31. A. P. Solon, J. M. Horowitz, Phase Transition in Protocols Minimizing Work Fluctuations. *Phys. Rev. Lett.* **120**, 180605 (2018), doi:10.1103/PhysRevLett.120.180605, <https://link.aps.org/doi/10.1103/PhysRevLett.120.180605>.
32. P. A. Erdman, A. Rolandi, P. Abiuso, M. Perarnau-Llobet, F. Noé, Pareto-optimal cycles for power, efficiency and fluctuations of quantum heat engines using reinforcement learning. *Phys. Rev. Res.* **5**, L022017 (2023), doi:10.1103/PhysRevResearch.5.L022017, <https://link.aps.org/doi/10.1103/PhysRevResearch.5.L022017>.
33. I. Prigogine, Introduction to thermodynamics of irreversible processes (1967).
34. S. R. de Groot, P. Mazur, Non-equilibrium Thermodynamics (Dover Publications) (1984).
35. G. Manzano, et al., Hybrid thermal machines: Generalized thermodynamic resources for multitasking. *Phys. Rev. Res.* **2**, 043302 (2020), doi:10.1103/PhysRevResearch.2.043302, <https://link.aps.org/doi/10.1103/PhysRevResearch.2.043302>.
36. L. Onsager, Reciprocal Relations in Irreversible Processes. I. *Physical Review* **37** (4), 405–426 (1931), doi:10.1103/PhysRev.37.405.
37. H. B. Callen, Thermodynamics and an Introduction to Thermostatistics (Wiley), 2nd ed. (1985).
38. C. Jarzynski, Equalities and inequalities: Irreversibility and the second law of thermodynamics at the nanoscale, in Time: Poincaré Seminar 2010 (Springer) (2012), pp. 145–172.
39. U. Seifert, From stochastic thermodynamics to thermodynamic inference. *Annual Review of Condensed Matter Physics* **10** (1), 171–192 (2019).
40. K. Proesmans, Y. Dreher, M. c. v. Gavrillov, J. Bechhoefer, C. Van den Broeck, Brownian Duet: A Novel Tale of Thermodynamic Efficiency. *Phys. Rev. X* **6**, 041010 (2016), doi:10.1103/PhysRevX.6.041010, <https://link.aps.org/doi/10.1103/PhysRevX.6.041010>.
41. Y.-H. Ma, D. Xu, H. Dong, C.-P. Sun, Universal constraint for efficiency and power of a low-dissipation heat engine. *Phys. Rev. E* **98**, 042112 (2018), doi:10.1103/PhysRevE.98.042112, <https://link.aps.org/doi/10.1103/PhysRevE.98.042112>.

42. P. Pietzonka, U. Seifert, Universal trade-off between power, efficiency, and constancy in steady-state heat engines. Physical Review Letters **120** (19), 190602 (2018), doi:10.1103/PhysRevLett.120.190602.
43. J. P. S. Peterson, et al., Experimental Characterization of a Spin Quantum Heat Engine. Phys. Rev. Lett. **123**, 240601 (2019), doi:10.1103/PhysRevLett.123.240601, <https://link.aps.org/doi/10.1103/PhysRevLett.123.240601>.
44. R.-X. Zhai, F.-M. Cui, Y.-H. Ma, C. P. Sun, H. Dong, Experimental test of power-efficiency trade-off in a finite-time Carnot cycle. Phys. Rev. E **107**, L042101 (2023), doi:10.1103/PhysRevE.107.L042101, <https://link.aps.org/doi/10.1103/PhysRevE.107.L042101>.
45. F.-M. Cui, H. Dong, Finite-Time Thermodynamics Perspective into Nuclear Power Plant Heat Cycle (2025), doi:10.48550/ARXIV.2509.25714, <https://arxiv.org/abs/2509.25714>.

Acknowledgments

Funding: We wish to acknowledge support from the CoQuSy project PID2022-140506NB-C21 and the María de Maeztu project CEX2021-001164-M for Units of Excellence, funded by MICIU/AEI/10.13039/501100011033/FEDER, UE. GM acknowledges the Ramón y Cajal program RYC2021-031121-I funded by MICIU/AEI/10.13039/501100011033 and European Union NextGenerationEU/PRTR. JAAM acknowledges Conselleria d’Educació, Universitat i Recerca of the Balearic Islands (Grant FPI_058_2022). We thank John Bechhoefer for fruitful discussions of optimization problems, and the corresponding authors of Refs. (12, 43, 40, 44, 45) for their consent of reproducing their experimental data in Fig. 3. All the research conducted and the entire writing of the manuscript were executed without using any large language modeling tool. Request for materials should be addressed to JAAM (joseantonio@ifisc.uib-csic.es).

Supplementary Materials for Pareto fronts and trade-off relations from exact multi-objective optimization of thermal machines

José A. Almanza-Marrero*, Édgar Roldán, Gonzalo Manzano

*Corresponding author. Email: joseantonio@ifisc.uib-csic.es

Supplementary Text

Mathematical details of the optimization process for endoreversible thermal machines

Herein, we provide the mathematical derivation for the solution of the multi-objective optimization problem. Our starting point is Eq. (6) in the main text, copied here for convenience

$$\Omega(\alpha, \beta, \gamma) = \alpha \bar{P} + \beta \bar{\eta} - \gamma \bar{\Sigma} - (1 - \alpha - \beta - \gamma) \overline{\sigma_p^2}. \quad (\text{S1})$$

Because the thermodynamic variables entering the optimization procedure are normalized (and the efficiency is normalized by definition), our goal is to optimize the values of the power P , entropy production Σ , and power variance σ_p^2 . We compute the *constrained* maximum values with respect to L_{11} and A_1 while maintaining L_{22} and A_2 fixed. We find that the constrained maximum values for the mean power, dissipation, and power fluctuations (efficiency is normalized by definition) are respectively given by

$$\begin{aligned} \max(P) &= \frac{1}{4} T A_2^2 L_{22}, \\ \max(\Sigma) &= A_2^2 L_{22}, \\ \max(\sigma_p^2) &= 2T^2 A_2^2 L_{22}. \end{aligned} \quad (\text{S2})$$

Equation (S2) leads to the following values of the thermodynamic normalized by their con-

strained maximum values

$$\begin{aligned}
\bar{P} &= \frac{4A_1 (A_2\sqrt{L_{11}L_{22}} - A_1L_{11})}{A_2^2L_{22}}, \\
\bar{\eta} &= \sqrt{\frac{L_{11}}{L_{22}} \frac{A_1}{A_2}}, \\
\bar{\Sigma} &= \frac{(A_1\sqrt{L_{11}} - A_2\sqrt{L_{22}})^2}{A_2^2L_{22}}, \\
\overline{\sigma_P^2} &= \frac{A_1^2L_{11}}{A_2^2L_{22}}.
\end{aligned} \tag{S3}$$

The optimization function given by Eq. (S1) reads, after substitution of Eq. (S3),

$$\Omega(\lambda) = \frac{A_2A_1\sqrt{L_{11}L_{22}}(4\alpha + \beta + 2\gamma) + A_1^2L_{11}(-3\alpha + \beta - 1) - A_2^2\gamma L_{22}}{A_2^2L_{22}}. \tag{S4}$$

By solving the parametric equation

$$\nabla_{A_1, L_{11}} \Omega(\lambda) = \left(\frac{\partial \Omega(\lambda)}{\partial A_1}, \frac{\partial \Omega(\lambda)}{\partial L_{11}} \right) = \mathbf{0}, \tag{S5}$$

we obtain the Pareto configurations, given by the relation

$$A_1 = \frac{A_2\sqrt{\frac{L_{22}}{L_{11}}}(4\alpha + \beta + 2\gamma)}{6\alpha - 2\beta + 2}. \tag{S6}$$

Substituting this value of the affinity into Eq. (S3), we obtain

$$\begin{aligned}
\bar{P} &= \frac{(2\alpha - 3\beta - 2\gamma + 2)(4\alpha + \beta + 2\gamma)}{(-3\alpha + \beta - 1)^2}, \\
\bar{\eta} &= \frac{4\alpha + \beta + 2\gamma}{6\alpha - 2\beta + 2}, \\
\bar{\Sigma} &= \frac{(2\alpha - 3\beta - 2\gamma + 2)^2}{4(-3\alpha + \beta - 1)^2}, \\
\overline{\sigma_P^2} &= \frac{(4\alpha + \beta + 2\gamma)^2}{(6\alpha - 2\beta + 2)^2}.
\end{aligned} \tag{S7}$$

Equation (S7) is not yet the physically-meaningful solution to the thermodynamically constrained optimization problem. In fact, since $\bar{\eta}$ is a linear function of A_1 [see Eq. (S3)], the optimal solution in Eq. (S7) may include “nonphysical” thermodynamic configurations where $\bar{\eta} > 1$, for example for the choice $\alpha = \gamma = 0$ and $\beta = 1$, for which we obtain $\bar{\eta} \rightarrow \infty$.

To enforce only physically meaningful configurations, the weight β associated with the efficiency should be such that when $\beta \rightarrow 1$, then $\bar{\eta} \rightarrow 1$. To ensure this, first we calculate the value of β for which the efficiency has physical values: if

$$\beta \leq 2(\alpha - \gamma + 1)/3, \quad (\text{S8})$$

then $\bar{\eta} \leq 1$. This condition is enforced by rescaling the efficiency's weight in Eq. (S7) as $\beta \rightarrow \beta^* = 2\beta(\alpha - \gamma + 1)/3$, leading to Eqs. (7)–(10) in the main text.

Bounding the performance for non-enderversible thermal machines

Here we provide explicit mathematical derivations of the results presented in Sec. 3.2 of the Main Text. We first introduce a set of dimensionless parameters that simplify the forthcoming formulae and derivations. First, we define the dimensionless parameter

$$x \equiv -\frac{A_1}{A_2} \sqrt{\frac{L_{11}}{L_{22}}} \geq 0, \quad (\text{S9})$$

and the dimensionless coupling coefficients

$$q_1 \equiv \frac{L_{12}}{\sqrt{L_{11}L_{22}}}, \quad q_2 \equiv \frac{L_{21}}{\sqrt{L_{11}L_{22}}}. \quad (\text{S10})$$

The power defined in Eq. (1) of the Main Text [$P = -T A_1 J_1$] may be written, using Eqs. (S9) and (S10), as a function of q_1 as

$$P(q_1) = TL_{22}A_2^2x(q_1 - x). \quad (\text{S11})$$

As discussed in the main text, the second law of thermodynamics requires the symmetric part of the Onsager matrix L_{ij} to be positive semi-definite, which implies the constraint

$$(q_1 + q_2)^2 \leq 4. \quad (\text{S12})$$

In the presence of microscopic reversibility—e.g., in the absence of magnetic fields or non-conservative forces—Onsager reciprocity holds, yielding $L_{12} = L_{21}$ which implies

$$q_1 = q_2 \equiv q. \quad (\text{S13})$$

Moreover, positivity of entropy production further implies

$$|L_{12}| \leq \sqrt{L_{11}L_{22}}. \quad (\text{S14})$$

Consequently, for any non-endoreversible thermal machine obeying Onsager reciprocity, $0 \leq q \leq 1$, while the endoreversible limit corresponds to perfect coupling, $q = 1$. In this case, the associated output power becomes

$$P_{\text{endo}}(q = 1) = TL_{22}A_2^2x(1 - x). \quad (\text{S15})$$

Subtracting Eqs. (S11) and (S15) gives

$$P_{\text{endo}}(q = 1) - P(q) = TL_{22}A_2^2x(1 - q). \quad (\text{S16})$$

Since by definition $1 - q \geq 0$, it follows that, for all $x \geq 0$, we get

$$P_{\text{endo}}(q = 1) \geq P(q \leq 1), \quad (\text{S17})$$

with equality only for $q = 1$ (endoreversible operation) or $x = 0$ (zero power).

We now discuss the efficiency, defined in Eq. (3) of the main text [$\bar{\eta} = -A_1J_1/A_2J_2$]. Expressing the fluxes in terms of the dimensionless variables introduced above, the entropy-producing flux reads

$$J_2 = L_{22}A_2(1 - q_2x), \quad (\text{S18})$$

where $1 - q_2x > 0$ and the inequality ensures the correct operation regime. The work-producing flux is

$$J_1 = \sqrt{L_{11}L_{22}}A_2(q_1 - x). \quad (\text{S19})$$

Using Eqs. (3), (S18), and (S19), the efficiency reads

$$\eta(q_1, q_2) = \frac{x(q_1 - x)}{1 - q_2x}, \quad x \geq 0, \quad 1 - q_2x > 0. \quad (\text{S20})$$

The condition $1 - q_2x > 0$ imposes $x < 1/q_2$; under Onsager reciprocity this reduces to the same operational range $x < 1$ as for the endoreversible machine. Evaluating Eq. (S20) at $q_1 = q_2 = 1$ yields the endoreversible efficiency

$$\eta_{\text{endo}}(q = 1) = \frac{x(1 - x)}{1 - x} = x, \quad 0 \leq x < 1. \quad (\text{S21})$$

From Eq. (S20), for $x > 0$ the inequality $\eta \leq x$ is equivalent to

$$q_1 \leq 1 + (1 - q_2)x. \quad (\text{S22})$$

Under Onsager reciprocity this condition becomes $q \leq 1 + (1 - q)x$, which is always satisfied in the operational regime since $q \leq 1$. Equality is attained only in the endoreversible case $q = 1$. Hence, the endoreversible thermal machine achieves, at every operating point x , the maximum efficiency allowed by linear irreversible thermodynamics under Onsager reciprocal relations.

We next show that the endoreversible thermal machine also provides a lower bound for the entropy production rate. Starting from the definition of the entropy production rate given in Eq. (2) of the main text [$\Sigma = A_1 J_1 + A_2 J_2$] and substituting $A_1 = -x A_2 \sqrt{L_{22}/L_{11}}$, we obtain

$$\Sigma(q_1, q_2) = L_{22} A_2^2 [1 - (q_1 + q_2)x + x^2]. \quad (\text{S23})$$

The endoreversible operation is again characterized by perfect coupling and Onsager reciprocity, i.e., $q = q_1 = q_2 = 1$. In this case,

$$\Sigma_{\text{endo}}(q = 1) = L_{22} A_2^2 (1 - x)^2, \quad (\text{S24})$$

which vanishes only in the reversible limit $x \rightarrow 1$. Subtracting Eq. (S24) from Eq. (S23) yields

$$\Sigma(q_1, q_2) - \Sigma_{\text{endo}}(q = 1) = L_{22} A_2^2 x (2 - q_1 - q_2). \quad (\text{S25})$$

Under Onsager reciprocity this simplifies to

$$\Sigma(q \leq 1) - \Sigma_{\text{endo}}(q = 1) = 2L_{22} A_2^2 x (1 - q), \quad (\text{S26})$$

since $0 \leq q \leq 1$ and $0 \leq x \leq 1$ in the operational domain, we conclude that

$$\Sigma(q \leq 1) \geq \Sigma_{\text{endo}}(q = 1), \quad (\text{S27})$$

for all $x \in [0, 1]$ with equality only for $q = 1$ (endoreversible operation) or $x = 0$. Thus, at every operating point x , the endoreversible thermal machine yields the minimal entropy production rate among all linear-response machines obeying Onsager reciprocal relations.

Finally, taking into account that fluctuations in the output power do not depend on the off-diagonal Onsager coefficients, together with our demonstration that endoreversible operation always bounds the performance of non-endoreversible machines satisfying Onsager symmetry, we conclude that the optimal Pareto fronts derived for endoreversible machines represent the ultimate performance limits for non-endoreversible reciprocal machines. We can relax the condition of Onsager symmetry and determine for which values of q_1 and q_2 the endoreversible operation still

bounds the non-endoreversible one. Starting from the condition on the power, we find that $q_1 \leq 1$. Using this condition together with the one in (S22), we also obtain $q_2 \leq 1$. The two conditions obtained so far, when considered together, also satisfy (S25).